

# Space-Time Accuracy Assessment of CFD Simulations for the Launch Environment

Jeffrey A. Housman\* and Michael F. Barad†

*Science and Technology Corporation, Moffett Field, CA 94035*

Cetin C. Kiris ‡

*NASA Ames Research Center, Moffett Field, CA 94035*

Time-accurate high-fidelity Computational Fluid Dynamics (CFD) simulations of the launch environment are an important part of the successful launch of new and existing space vehicles. The capability to accurately predict certain aspects of the launch environment, such as ignition overpressure (IOP) waves and launch acoustics, is paramount to mission success. Implicit dual-time stepping methods represent one approach to provide accurate computational results in a timely manner. Two simplified test cases related to the launch environment are examined. The first test case models the IOP waves generated from a 2D planar jet located above a 45-degree flat plate, while the second case investigates launch acoustic noise generated from the jet of a rocket impinging on an axisymmetric flame trench and mobile launcher. Sensitivity analysis has been performed and a verification procedure was applied to investigate the necessary spatial and temporal resolution requirements for CFD simulations of the launch environment using an implicit dual-time method.

## Nomenclature

$\Delta t$	Time-step size (s)	$\Delta x$	Spatial-step size (m)
$\epsilon$	Sub-iteration convergence criteria	$T_{ref}$	Reference temperature (K)
$U_{ref}$	Reference velocity (m/s)	$P_{ref}$	Reference pressure (Pa)
$C_p$	Specific heat at constant pressure (J/kg/K)	$\gamma$	Ratio of specific heats
HLV	Heavy Lift Vehicle	ML	Mobile Launcher
IOP	Ignition Overpressure	DOP	Duct Overpressure
CFD	Computational Fluid Dynamics	CAA	Computational Aeroacoustic Analysis
RMS	Root-Mean-Squared	SRB	Solid Rocket Booster

## I. Introduction

The National Aeronautics and Space Administration (NASA) is currently exploring new options for future space vehicles, including Heavy Lift Vehicles (HLV) to carry large payloads to low-earth-orbit and beyond. The HLVs will require much higher thrust than current launch vehicles. Using larger, more powerful solid rocket boosters (SRBs) is one option being considered to provide the additional thrust. The feasibility of launching HLVs from the existing facility at Kennedy Space Center (KSC) must be considered. Due to the increased thrust, several problems must be addressed. Two such problems are the assessment of the water suppression system to reduce the Ignition Overpressure (IOP) waves and characterization of the launch acoustic environment.

Upon ignition of the solid rocket propulsion system, large-magnitude IOP waves are generated during the buildup of thrust, in which mass is suddenly injected from the nozzle through the exhaust holes of the

---

\*Research Scientist, Applied Modeling and Simulation Branch, NAS Division, MS N258-2; Jeffrey.A.Housman@nasa.gov.

†Research Scientist, Applied Modeling and Simulation Branch, NAS Division, MS N258-2; Michael.F.Barad@nasa.gov.

‡Branch Chief, Applied Modeling and Simulation Branch, NAS Division, MS N258-2; Cetin.C.Kiris@nasa.gov.

Copyright © 2011 by the American Institute of Aeronautics and Astronautics, Inc. The U.S. Government has a royalty-free license to exercise all rights under the copyright claimed herein for Governmental purposes. All other rights are reserved by the copyright owner.

mobile launcher into the confined volume of the flame trench. The additional mass displaces the air in the trench, causing a piston-like action in which compression and expansion waves travel between the mobile launcher and the flame trench. The reflected IOP waves can travel back towards the launch vehicle and potentially affect structural integrity. The IOP waves can also affect the stability of the vehicle during the first second of launch, and could generate a dangerous debris field. In order to reduce the magnitude of the IOP waves, a water suppression system has been established, in which jets of water are injected into the exhaust plume. Predicting the magnitude and direction of the IOP waves generated by HLVs is critical to assess the effectiveness of the water suppression system.

Once the IOP waves have subsided and the vehicle is ascending, launch acoustics become critical. Launch acoustics are characterized by small amplitude pressure waves with broadband sound pressure levels. During launch, acoustic noise is generated by the turbulent exhaust jet mixing with the ambient air and impinging on the flame trench. The transient acoustic waves cause structural vibrations which can adversely affect the payload and electronics of the vehicle, as well as tower operations. Accurate prediction of the noise generation mechanisms and sound propagation can be used to ensure payload safety.

High-fidelity time-accurate Computational Fluid Dynamics (CFD) simulations have been established as a central component in the safety assessment of launch vehicles both during takeoff and throughout the mission.<sup>1-3</sup> The ability to predict specific phenomenon such as IOP waves and launch acoustics is critical to the successful launch of a vehicle. One method to provide accurate results for unsteady fluid dynamic problems, using a reasonable amount of computational resources, is the dual-time stepping method. The dual-time stepping method is an implicit numerical method for unsteady flows in which a pseudo-time process is embedded into each physical time-step and the discrete nonlinear system is marched to a pseudo-steady state.<sup>4</sup> Originally developed to extend the artificial compressibility method to unsteady incompressible flows, the dual-time procedure allows efficient steady-state convergence algorithms to be applied at each physical time-step. Another important advantage of dual-time stepping methods is numerical stability, allowing the user to choose the time-step based on the relevant physics of the problem.

While time-accurate CFD simulations offer a powerful prediction tool for modeling unsteady flows, it is often difficult to determine the required spatial and temporal resolution requirements as well as quantifying the error in the computed results. For example, it has been shown that using excessively large time-steps combined with incomplete convergence of the sub-iteration procedure may generate spurious solutions that appear physically reasonable but contain large amplitude and phase errors.<sup>5</sup> Currently, no well-established theory exists on necessary conditions (i.e. number of sub-iterations, residual convergence, etc.) to maintain a specified space-time accuracy. One could simply perform sub-iterations until machine convergence is achieved for each time-step, but this is not computationally economical for the accuracy requirements of most engineering applications. Often, a grid, time-step, and number of sub-iterations is chosen based on intuition or expert knowledge about the problem. Although this approach may be perfectly adequate it lacks rigorous mathematical justification. A verification procedure of the dual-time stepping method is described to determine the requirements for modeling launch environment flows. Time-step convergence of application specific functionals on a fixed mesh is demonstrated. Space-time convergence of these functionals is shown to be more difficult to achieve.

## I.A. Objectives and Approach

The objectives of this work are to determine the spatial and temporal resolution requirements to accurately model the launch environment, and develop a procedure to assess the accuracy of the unsteady simulations when experimental and flight data do not exist. Specifically, the simulation of IOP waves during ignition and the noise generation and sound propagation associated with launch acoustics. Results of this study will be used as a guideline in selecting an appropriate grid resolution and time-step for future launch applications.

In order to fulfill the objectives, two simplified inviscid model problems are proposed to represent the launch environment. The first is a 2D jet impinging on a flat plate at 45-degrees, which represents IOP wave phenomenon. The second is an rocket launching from an idealized mobile launcher above a flame trench. The entire domain is represented by a single plane axisymmetric assumption and appropriate source terms are included in the governing equations. The rocket is located far above the launcher and longer time integration is performed to identify the launch acoustics properties. Detailed sensitivity analysis of the unsteady pressure signatures to both mesh size and time-step is performed. Results from the analysis are used in a dual-time verification procedure to assess the accuracy of the simulations. Although the model problems exclude 3D effects, they still retain much of the physical complexity of the true applications, while

having computational requirements small enough to perform the large sensitivity analysis and verification study.

### I.B. Dual-time Verification Procedure

The dual-time verification procedure consists of a two-step process. Before the procedure is described, two convergence criteria are defined:

- TIME-STEP CONVERGENCE, defined by fixing the spatial mesh and sub-iteration convergence criteria, and determining the time-step required for the solution to converge with respect to a predefined measure.
- SPACE-TIME CONVERGENCE, defined by fixing the sub-iteration convergence criteria, and determining the spatial and temporal resolution required for the solution to converge with respect to a predefined measure. In this case mesh spacing and time-step are linked such that  $\Delta x \propto \Delta t$ .

In the definitions above, the term "converge with respect to a predefined measure", means that the change of some measure of the solution becomes smaller than a user defined tolerance. For example, the measure could be the time integral of pressure at a specific point, or the  $L2$ -norm of the difference between two solutions. Definitions of the measure and the convergence tolerance are problem dependent, and should be chosen to assess the simulation's accuracy for each particular application.

The first step of the verification procedure consists of determining time-step convergence for a fixed mesh. Starting on a coarse mesh, the unsteady solution is computed using a sequence of monotonically decreasing time-steps. Once the solution has converged with respect to the predefined measure (i.e. the functional stops changing with decreasing time-step), time-step convergence has been achieved. Unsteady solutions are then computed on a finer mesh with a subset of the monotonic sequence of time-steps used on the previous mesh. This procedure continues until time-step convergence is achieved on each relevant mesh, at which point the largest time-step to maintain a prescribed temporal accuracy level for each fixed mesh resolution is obtained.

The second step of the verification procedure builds on the results of the first step. Examining the results of the time-step convergence analysis for each level, a particular combination of time-step and spatial resolution are chosen. Holding the ratio of  $\Delta t/\Delta x$  fixed, the functional is plotted for a sequence of meshes with monotonically increasing resolution. Once the functional stops changing with increasing resolution (within a user-prescribed tolerance), space-time convergence has been achieved. Note if the space-time convergence criteria is not satisfied, the analysis can still be used to provide a reasonable error estimate of the solution.

## II. Computational Methodology

A 2D/3D CFD code, LAVA (Launch Ascent and Vehicle Aerodynamics), using the dual-time stepping method is applied. The numerical method has options for both overset and immersed boundary spatial discretizations with block-structured adaptive mesh refinement. Details of the governing equations and discretization are omitted, see References<sup>6-8</sup> for the overset formulation. Second-order backward differencing is used in time and a preconditioned formulation of the Roe numerical flux for the convective terms. Higher-order accuracy in space is obtained using standard MUSCL extrapolation of the primitive variables with the MINMOD limiter to control numerical oscillations at shocks. A domain decomposition approach is used for parallel computation, implemented using the MPI standard for parallel communication.

In the overset grid methodology, as described in Reference,<sup>9</sup> the solution domain is decomposed into overlapping patches (or zones) of body-fitted curvilinear grids. The overlapping grids must be assembled such that points which reside inside the solid bodies are removed from the domain (blanked) and points that require boundary information are identified and filled with interpolation. Figure 3 shows an example of the overset grid assembly process. The governing equations are transformed to curvilinear coordinates in strong conservation law form.<sup>10</sup> Next, the transformed equations are discretized on each individual zone where the boundary of the zone is updated through either physical boundary conditions or overset interpolation from an overlapping donor zone. Second-order accurate interpolation is used on overlapping boundaries to maintain the overall accuracy of the method. The linear system of equations, which must be solved at each sub-iteration, is relaxed using an alternating line-implicit Jacobi procedure.

In the immersed boundary methodology, complex 3D geometries are discretized using a sharp interface immersed boundary method (IB), similar to Reference<sup>11</sup>. In this method, boundary conditions are imposed on the Cartesian grid by extending the solution into the body. This results in a method that is accurate and free of small-cell stability problems. For the bulk of the flow, which is  $O(N)$  control volumes, we compute on a regular Cartesian grid composed of rectangular parallelepiped (or cuboid) cells. We use the immersed description for the  $O(N^{\frac{D-1}{D}})$  cells that intersect the boundary, where  $D$  is the dimension. The launch environment contains a wide range of both spatial and temporal scales. In order to simulate this range of spatial scales, a multi-resolution numerical method is required. Adaptive mesh refinement (AMR) is a proven methodology for multi-scale problems with an extensive existing mathematical and software knowledge base. The LAVA code has been extended using the high-performance Chombo AMR library<sup>12</sup> to provide a multi-resolution capability that can coarsen and refine as a simulation progresses. An example showing the 3D IB-AMR capabilities of LAVA for a complex launch environment is shown in Figure 1 and 2. These figures illustrate IOP waves generated from Solid Rocket Boosters (SRBs) during the launch of a HLV. The 3D simulations are computationally expensive, therefore space-time accuracy assessment are performed on 2D representative problems to determine resolution requirements.

### III. Results and Analysis

#### III.A. Ignition Overpressure Problem

The IOP model problem was jointly defined by NASA and the Japan Aerospace Exploration Agency (JAXA) through a collaborative agreement. The geometry for the IOP wave propagation problem consists of a 2D rocket nozzle located above a 45-degree flat plate, as shown in Figure 4(a). The nozzle exit diameter is 0.1 meters and is located 0.5 meters above the plate. Unsteady stagnation conditions are prescribed at the nozzle plenum, where the dimensionless stagnation pressure is shown in Figure 4(b) and the stagnation temperature is held fixed at the reference temperature  $T_{ref} = 300$  K (cold jet). The remaining reference conditions are: pressure  $P_{ref} = 100$  kPa, velocity  $U_{ref} = 0$  m/s, specific heat at constant pressure  $C_p = 1005$  J/kg/K, and the ratio of specific heats  $\gamma = 1.4$ . Slip-wall boundary conditions are used on the nozzle walls and on the plate for inviscid simulations. The far-field grid is extended away from the region of interest so that the IOP wave never leaves the solution domain within the time integration limits. Fourteen point locations were selected in the domain of interest, as shown in Figure 4(a), and the time history of pressure at each of these locations is recorded. Since the purpose of simulating IOP wave phenomenon is to assess the peak pressure values (both suction and load), the application dependent functional chosen for the dual time verification procedure is the magnitude of the gauge pressure at each selected point location. For each sample point, this functional is mathematically defined as

$$F(p) = \max_{0 \leq t \leq T} |p(t) - P_{ref}|. \quad (1)$$

Similar results were obtained at each of the selected point locations, so only the results at point location 6 are reported.

Three mesh resolutions were generated for the present analysis. Figures 5(a)–(d) show the entire domain, a diagram of the overlapping grid system, and two different views of the coarse resolution overset grid. The finest off-body mesh spacing  $h$  for each mesh resolution is chosen to match the outer boundary spacing of the near-body grids;  $h = \Delta x = 0.005m$  (Coarse),  $h = \Delta x/2$  (Medium), and  $h = \Delta x/4$  (Fine). Table 1 displays the number of zones, number of points, and number of CPU cores used for the simulations. A total of 10 cases were run on the coarse grid with physical time-steps corresponding to CFL = 0.5, 1, 2, 4, ... , 256, and 16 orders of magnitude reduction in the residual at each time-step was required for  $0 < t < 100 \cdot D_{exit}/C_{ref} = 0.028796$  seconds. A total of five physical time CFLs were chosen from this set and used to perform simulations on the medium and fine grids, in which 16 orders of magnitude reduction in the residual at each time-step was again required. By removing the solution dependence on sub-iteration convergence criteria, the largest physical time-step which remains accurate to engineering tolerances was chosen for each grid level. In order to reduce computational costs further, the medium mesh with CFL = 4 was chosen to perform a sensitivity analysis with respect to convergence criteria. An additional four cases are run with convergence tolerances of 1, 2, 4, and 8 orders of magnitude residual reduction. This resulted in 24 total unsteady cases which required approximately 2 days to complete on NASA Advanced Supercomputing (NAS) Division’s *Pleiades* supercomputer.

Resolution	Zones	Points	Cores
Coarse	24	165k	8
Medium	66	552k	24
Fine	209	1,945k	120

Table 1. Grid statistics and processor usage for the IOP test case.

A constant physical time-step is used throughout the simulations which was set with a prescribed CFL number by

$$\Delta t = \frac{CFL \ h}{\lambda_{max}}. \quad (2)$$

In Equation 2 the velocity speed  $\lambda_{max} \approx 788$  m/s which is an approximation of the maximum wave speed determined from steady Quasi-1D nozzle theory. This should not be confused with the typical time-step definition used in explicit algorithms where  $h$  is the smallest spacing in the grid and  $\lambda_{max}$  is the maximum wave speed in the entire domain at the current time. The explicit time-step definition leads to orders of magnitude smaller time-steps and changes the time-step throughout the simulation. This would require a modified implementation of the second-order backward difference scheme.

In Figure 6 an unsteady time-sequence of the gauge pressure (psig) is shown to illustrate the physics of IOP wave initiation and propagation. Initially, high pressures are generated as the thrust builds up. Next, low pressure is created aft of the nozzle throat caused by choking and strong vortex waves are observed in the shear layer of the jet. Once the jet impinges on the plate, strong waves are reflected. As time increases diamond structures form in the jet and acoustic wave structures are observed throughout the domain of interest. Assessing the accuracy of the unsteady simulations is described in the next two sub-sections, and computational efficiency is addressed in the final sub-section.

### III.A.1. Time-Step Sensitivity Analysis

Unsteady simulations were first computed on the coarse mesh for 10 distinct time-steps ranging from  $8.0e-4 - 1.6e-6$  seconds. A time history of the dimensionless gauge pressure at point location 6 for each of the  $CFL$  conditions is plotted on Figure 7(a). The largest time steps associated with  $CFL = 128$  and  $256$  are noticeably diffused, but it is hard to distinguish differences between the pressure signatures generated using the smaller time-steps. In order to quantitatively assess the sensitivity of the solution to time-step the functional defined in Equation 1 is plotted versus time-step at point location 6 along with the estimated temporal error in Figures 7(b) and (c). The estimated error is computed as the difference between the functional predicted using an intermediate time-step with the functional predicted using the finest time step. Examining the plots it is observed that the functional value is *time-step converged* for  $CFL \leq 8$ . This suggest that using a  $CFL = 8$  is sufficient for simulating IOP wave physics on the coarse mesh. It does not indicate whether the coarse mesh itself is sufficiently accurate. Continuing with the verification procedure, unsteady simulations were performed on the medium resolution mesh for  $CFL = 0.5, 1, 2, 4,$  and  $8$ . Focusing on location 6, Figure 7(d) plots the time-history of dimensionless gauge pressure. These pressure signatures are indistinguishable from one another, which is confirmed by the functional convergence history and error estimate plotted in Figures 7(e) and (f). This suggests the  $CFL = 8$  remains sufficient, but we remark that the actual time-step has been reduced by a factor of 2 between the coarse and medium mesh resolutions. Finally, the unsteady simulations are performed on the fine mesh using the aforementioned  $CFL$  numbers. In this case, differences are observed in the time-history at location 6 when using  $CFL = 8$  between  $0.014 \leq t \leq 0.015$ (s), where a larger positive gauge pressure is observed at two different peaks in Figure 7(g). Examining the functional convergence and error estimate plots in Figures 7 (h) and (i), an error of approximately 1.55% is estimated for the  $CFL = 8$  simulation. This estimate should not be mistaken for an actual error between the numeric functional and the functional evaluated with the exact solution of the governing equations. The estimate is simply the sensitivity of the functional to the time-step on a fixed mesh. A more rigorous error estimate was performed in the next sub-section. From the time-step sensitivity analysis a  $CFL = 4$  appears both accurate, economical, and conservative for the mesh resolutions included in the study.

### III.A.2. Space-Time Sensitivity Analysis

The second step of the dual time verification procedure is to analyze the sensitivity to space-time resolution. From the results of the time-step sensitivity analysis the unsteady solution computed on each mesh level with a time-step associated with  $CFL = 4$  are used to perform the space-time sensitivity analysis. Figure 8(a) plots the time history of dimensionless gauge pressure at location 6 for each mesh level. It is observed that higher frequency wave content is captured as the spatial and temporal resolution increases. Second, the suction pressure appears to have two peaks that are very close in magnitude. The first peak appears smooth and well-resolved on each mesh, while the second peak appears after the onset of small scale acoustic effects. This might have affected the space-time functional convergence if finer grids are included in the study. The space-time functional convergence is analyzed in Figures 8(b) and (c) which plots the functional value versus mesh size  $h$  along with a log-log plot of the difference between the functional predicted on the coarse and medium meshes with the fine mesh. The difficulty in achieving true space-time convergence is evident, the functional values are clearly increasing with finer mesh resolution. With that said, the percent error between the functional values predicted on the fine and medium meshes is below 5% (the black dashed horizontal line) which is a reasonable engineering tolerance for such complicated physical phenomenon. It is also observed that the error is reducing at almost second-order (blue dashed line is second order slope while red dashed line is first-order). This is promising considering the highly nonlinear nature of the flow which includes many shock waves and contact discontinuities. Overall the medium mesh resolution with  $CFL = 4$  appears to be an adequate choice for simulating IOP waves.

### III.A.3. Convergence Tolerance Analysis

The dual time verification procedure, consisting of time-step and space-time sensitivity analyses, has provided quantitative evidence indicating sufficient spatial and temporal resolution requirements for modeling IOP waves. In the previous analysis the coupled nonlinear system of equations were solved at each time-step using a 16-order of magnitude residual reduction criteria. This is very severe, and not necessary for maintaining the solution accuracy. In order to determine a more economical convergence criteria, while maintaining the accuracy of the simulation, a convergence tolerance study is performed. The unsteady simulation is computed using the medium mesh and  $CFL = 4$  with residual reduction tolerances of 1, 2, 4, and 8 orders of magnitude. The time history and functional sensitivity to convergence tolerance are used to assess the accuracy of the simulations. In this study the error estimated using the functional value predicted using the 16-orders of magnitude residual reduction results previously computed. Large phase and amplitude errors are observed in the time history plot, shown in Figure 9(a), when the nonlinear residual is only converged one to two orders of magnitude at each time-step. Examining the functional convergence and error estimate plots in Figure 9(b) and (c), four orders of magnitude convergence in residual appears sufficient to maintain an engineering level accuracy.

## III.B. Launch Acoustic Problem

### III.B.1. Problem Setup

After determining relevant spatial and temporal resolution requirements for simulating IOP wave phenomenon, a similar dual time verification procedure was applied to a model launch acoustic problem. The launch acoustic model problem was designed to assess the capability of the dual-time stepping method in capturing noise generation and sound propagation. The geometry of the problem consists of a fictitious axisymmetric launch site containing a generic rocket, mobile launcher (ML), and flame trench as shown in Figure 10(a). This domain is represented using a single-plane and axisymmetric source terms are included in the governing system of equations. Twenty-seven point locations were selected for recording the unsteady pressure history, which are shown in 10(b). Identical reference conditions as those described above are used for this case. The interior of the nozzle is not modeled, and a steady supersonic nozzle exit profile is imposed on the nozzle exit, see Reference<sup>13</sup> for details. As in the previous case, slip-walls are used for the rocket, mobile launcher, and flame trench. The far-field is also extended far away from the rocket and extremely coarse meshes are used in the far-field to sufficiently dissipate the pressure waves before they reach grid boundaries, avoiding spurious reflections.

Four mesh resolutions were generated for the launch acoustic problem, and a diagram of the overlapping grid system is shown in the upper right corner of Figure 10(a). The finest off-body mesh spacing  $h$  for each

grid resolution (again chosen to match the outer boundary spacing of the near-body grids) and the time steps used for the CFD runs were:

- COARSE:  $h = \Delta x = 0.15m$  and eight time steps ranging from  $3.20 \times 10^{-4} \leq \Delta t \leq 2.50 \times 10^{-6}$  seconds.
- MEDIUM:  $h = \Delta x/2$  and eight time steps ranging from  $8.00 \times 10^{-5} \leq \Delta t \leq 6.25 \times 10^{-7}$  seconds.
- FINE:  $h = \Delta x/4$  and seven time steps ranging from  $4.00 \times 10^{-5} \leq \Delta t \leq 6.25 \times 10^{-7}$  seconds.
- ULTRA-FINE:  $h = \Delta x/8$  and six time steps ranging from  $2.00 \times 10^{-5} \leq \Delta t \leq 6.25 \times 10^{-7}$  seconds.

Dimensional time-steps are listed above, instead of the *CFLs* used in the previous analysis. Each case was simulated for one second of physical time with a convergence criteria of 16 orders of magnitude reduction in the global  $L2$  norm of the residual at each physical time-step. This eliminated incomplete sub-iteration convergence from the analysis, as was done for the IOP problem. Table 2 displays the number of zones, number of points, and number of CPU cores used for the overset method.

Resolution	Zones	Points	Cores
<b>Coarse</b>	59	171k	8
<b>Medium</b>	102	503k	24
<b>Fine</b>	247	1,603k	84
<b>Ultra-Fine</b>	674	5,484k	264

Table 2. Grid statistics and processor usage for the launch acoustic test case.

A time sequence of the gauge pressure showing the initiation and propagation of the launch acoustics is displayed in Figure 11. For the acoustic simulations the rocket is held stationary at 60.96 m. above the mobile launcher. Since the time scale of the launch acoustics is much smaller than the time it takes a rocket to travel away from the launch facility, this assumption should be valid (at least over some specific time interval). Before the acoustic behavior of the flow field is considered, the initial transient pressure waves must pass out of the domain of interest. This initial wave is seen in the first two images of the sequence, ( $t = 0.256$  and  $0.512$  s). Once the initial transient has subsided, the jet impinging on the trench and interacting with the mobile launcher creates a phenomenon called Duct Overpressure (DOP). The DOP waves travel back up the hole of the mobile launcher and out of the sides between the launcher and the flame trench, ( $t = 0.768$  and  $1.000$  s). Along with the DOP waves, the jet creates lower amplitude sound waves, known as Mach waves, which interact with the DOP waves and the launch structure. These simulations are intended to capture the generation, reflection, and interaction of the acoustic waves, all within an idealized axisymmetric simulation in order to assess the resolution requirements for 3D simulations.

In order to apply the dual time verification procedure and quantify the accuracy of the launch acoustic simulations, a functional associated with sound pressure level is used. In this case, the Root-Mean-Squared (RMS) functional of gauge pressure is chosen as the application dependant functional,

$$F_{RMS}(p) = \left[ \frac{1}{(T_2 - T_1)} \int_{T_1}^{T_2} (p(t) - P_{ref})^2 dt \right]^{\frac{1}{2}}. \quad (3)$$

The two time instances used in the functional are,  $T_1 = 0$  and  $T_2 = 1.0$ . Although this time interval is too short for extracting relevant sound pressure levels, acoustic effects appear to dominate the pressure signature after 0.5 seconds.

### III.B.2. Time-Step Sensitivity Analysis

The axisymmetric launch acoustic test case analysis was more computationally expensive than the IOP test case due to the longer time integration and the additional mesh resolution. The computational cost the ultra-fine mesh resolution and smallest time-step was approximately 10 days of continuous runtime using 264 cores. Results from this study are shown for point locations 9 and 12 which are located on the payload section of the generic rocket and on the bottom corner (jet side) of the ML, see Figure 10. Figure 12(a)–(i) shows the time history of dimensionless gauge pressure, the functional convergence history, and the temporal

error estimates for the coarse, medium and fine mesh resolutions at point location 9. As the spatial resolution increases, higher frequency wave content is captured (though under-resolved) as expected from the broadband nature of launch acoustics. The qualitative features such as the larger IOP and DOP waves appear to be captured, but larger variations in the small amplitude waves are observed as the mesh and time-step are refined. Examining the functional history and temporal error estimates, *time-step convergence* is achieved on the coarse and medium mesh resolutions, but not on the fine mesh resolution. The same observations are made at point location 12 where Figure 13(a)–(i) shows the time history of dimensionless gauge pressure, the functional convergence history, and the temporal error estimates for the coarse, medium and fine mesh resolutions. Comparing the time and functional histories, it appears that point location 9 contains less high frequency wave content in the pressure history and is better behaved with respect to percent error with decreasing time-step. This makes sense since location 9 is in a region where acoustic waves are propagated to, while location 12 is in a noise generating region of the domain. This distinction of how well the current CFD tools predict noise generating and acoustic propagation regions will be elaborated in the next section. Overall it appears that *time-step convergence* is difficult to achieve for the launch acoustic problem as the mesh is refined.

### III.B.3. Space-Time Sensitivity Analysis

Once the initial 23 unsteady simulations were completed for the coarse, medium, and fine grids and the time-step sensitivity analysis was performed, an additional ultra-fine grid was generated and 6 unsteady simulations were performed in order to assess the space-time sensitivity of the RMS functional for the launch acoustic problem. From these results the fixed ratio  $\Delta t/\Delta x = 1/15260$  is chosen and the time history, functional history, and space-time error estimate for point locations 9 and 12 are compared in Figures 14(a)–(f). The time-histories plotted in Figures 14(a) and (d) show that additional high frequency information is captured at both point locations as the resolution is increased in both space and time. Phase differences are also evident at location 9 after 0.4 seconds. Similar to the IOP results of the space-time sensitivity analysis the functional history at location 9 appears to be trending toward a converged value, but is not converged in space-time. The functional history at location 12 is much worse, showing no sign of convergence in space-time. In fact the error estimate appears to be increasing with resolution. This analysis suggests that noise generating regions may be too energetic to converge using the present definition. It may be necessary to redefine the functional such that only certain frequencies in time are included in the RMS functional. In general it does not appear that the dual time stepping method with second-order (space and time) upwind schemes are capable of achieving space-time convergence nor engineering level accuracy for launch acoustic problems throughout the domain. These methods may be used in conjunction with linearized aeroacoustic tools in a hybrid fashion, which is one of the paths of future work the authors are examining. Alternatively, higher-order and/or adaptive methods may be promising.

## IV. Conclusion

A dual-time stepping method has been applied to two launch environment test cases. A large parameter study was presented examining the sensitivity of unsteady pressure history to time-step and mesh size. A dual time verification procedure was developed to assess the accuracy of the simulations (since no experimental or flight data exists for these cases). Time-step convergence on a fixed mesh was demonstrated for the IOP wave problem and on the coarse and medium mesh of the launch acoustic problem. Space-time convergence analysis was performed and the selected functionals do not appear to be converged indicating that additional refinement (much finer than practical for 3D simulations) is required. Space-time error estimates below 5% tolerance level are achieved for the IOP problem but not the launch acoustic problem. Study of the space-time convergence properties of the dual-time stepping method applied to launch environment flows is ongoing. Pure CFD analysis for launch acoustic flows is expensive and under-resolved. Future efforts in modeling launch acoustics will focus on investigating hybrid approaches using empirical information, analytic methods, and computational aeroacoustic analysis (CAA) in conjunction with CFD results.

# Acknowledgments

## References

- <sup>1</sup>Kiris, C., Housman, J., Gusman, M., Chan, W., and Kwak, D., “Time-Accurate Computational Analysis of the Flame Trench Applications,” *21st Intl. Conf. on Parallel Computational Fluid Dynamics*, 2009, pp. 37–41.
- <sup>2</sup>Kiris, C., Kwak, D., Chan, W., and Housman, J., “High-fidelity simulations of unsteady flow through turbopumps and flowliners,” *Computers & Fluids*, Vol. 37, 2008, pp. 536–546.
- <sup>3</sup>Gomez, R., Vicker, D., Rogers, S., Aftosmis, M., Chan, W., Meakin, R., and Murman, S., “STS-107 Investigation Ascent CFD Support,” *34th AIAA Fluid Dynamics Conference and Exhibit, Portland, Oregon*, June 28 - July 1, 2004, AIAA-2004-2226.
- <sup>4</sup>Rogers, S.E. and Kwak, D. and Kiris, C., “Steady and Unsteady Solutions of the Incompressible Navier-Stokes Equations,” *AIAA Journal*, Vol. 29, No. 4, April 1991, pp. 603–610.
- <sup>5</sup>Housman, J., Barad, M., Kiris, C., and Kwak, D., “Space-Time Convergence Analysis of a Dual-Time Stepping Method for Simulating Ignition Overpressure Waves,” *ICCFD6, July 12-16, St. Petersburg, Russia*, 2010.
- <sup>6</sup>Housman, J., Kiris, C., and Hafez, M., “Preconditioned Methods for Simulations of Low Speed Compressible Flows,” *Computers & Fluids*, 2009, In Print (Available Online).
- <sup>7</sup>Housman, J., Kiris, C., and Hafez, M., “Time-Derivative Preconditioning Methods for Multicomponent Flows - Part I: Riemann Problems,” *Journal of Applied Mechanics*, Vol. 76, No. 2, February 2009.
- <sup>8</sup>Housman, J., Kiris, C., and Hafez, M., “Time-Derivative Preconditioning Methods for Multicomponent Flows - Part II: Two-Dimensional Applications,” *Journal of Applied Mechanics*, Vol. 76, No. 3, March 2009.
- <sup>9</sup>Steger, J. and Benek, J., “On the Use of Composite Grid Schemes in Computational Aerodynamics,” Technical Memorandum 88372, NASA, 1986.
- <sup>10</sup>Vinokur, M., “Conservation Equations of Gasdynamics in Curvilinear Coordinate Systems,” *Journal of Computational Physics*, Vol. 14, 1974, pp. 105–125.
- <sup>11</sup>Ghias, R., Mittal, R., and Dong, H., “A Sharp Interface Immersed Boundary Method for Compressible Viscous Flows,” *Journal of Computational Physics*, Vol. 225, July 2007, pp. 528–553.
- <sup>12</sup>Colella, P., Graves, D. T., Ligocki, T. J., Martin, D. F., Modiano, D., Serafini, D. B., and Straalen, B. V., “Chombo Software Package for AMR Applications - Design Document,” unpublished.
- <sup>13</sup>Gusman, M., Housman, J., and Kiris, C., “Best Practices for CFD Simulations of Launch Vehicle Ascent with Plumes - OVERFLOW Perspective,” *49th AIAA Aerospace Sciences Meeting, Orlando, Florida*, Jan 4–7 2011, AIAA-2011-1054.

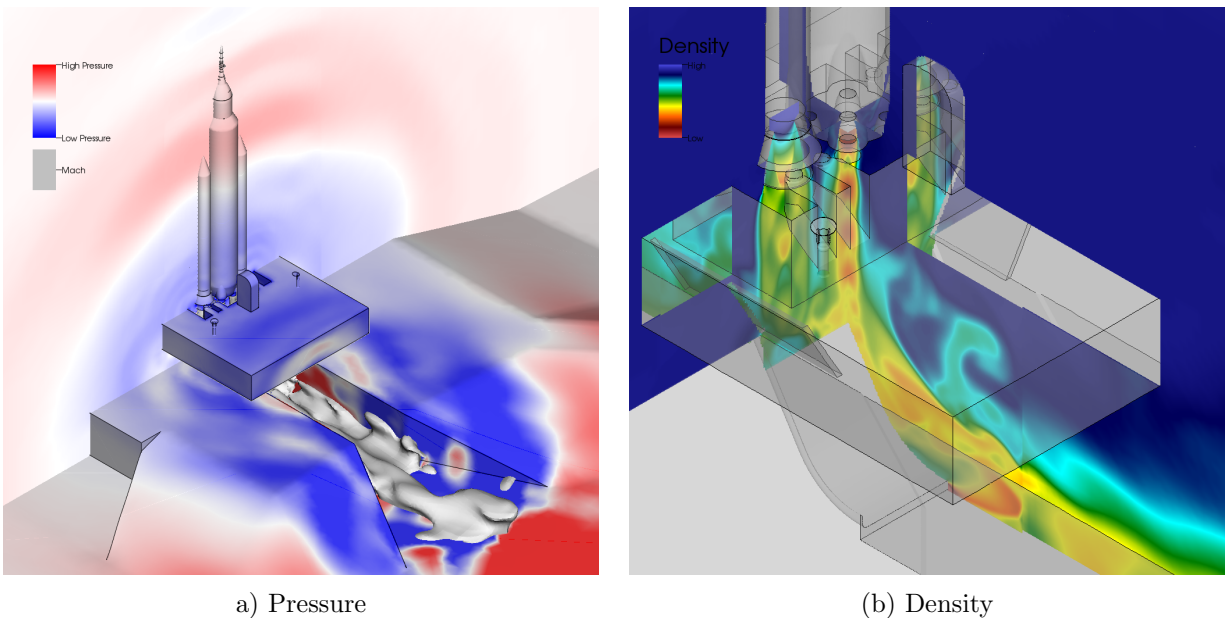


Figure 1. (a) Gauge pressure showing IOP, (b) zoom in on density slices, both for a realistic launch vehicle. Simulated with the LAVA code using the IB-AMR method.

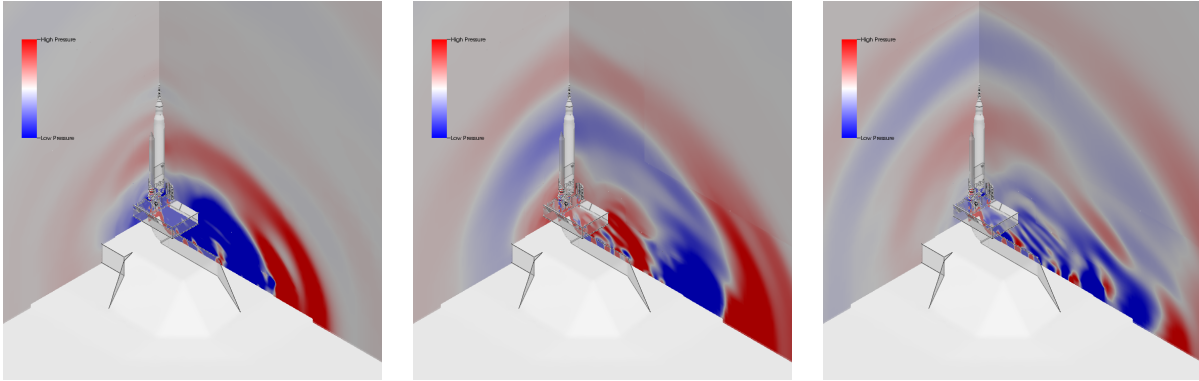


Figure 2. Time sequence of gauge pressure, showing IOP wave physics for a realistic launch vehicle. Simulated with the LAVA code using the IB-AMR method.

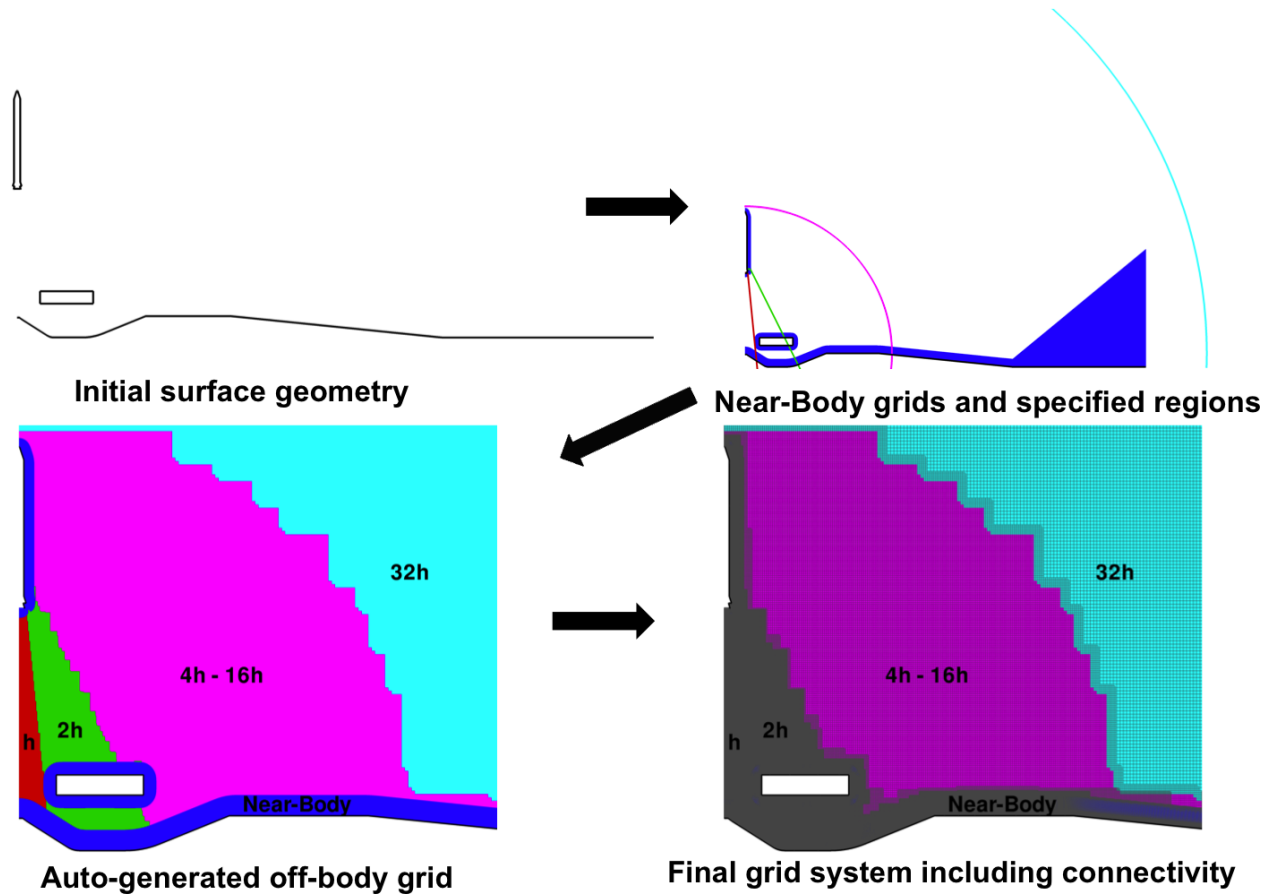


Figure 3. Overset grid generation procedure: Step 1, define the underlying surface geometry; step 2, generate body-fitted near-body grids and define specified regions of interest; step 3, automatically generate off-body Cartesian grids to fill the domain, provide sufficient overlap for proper connectivity and resolve the specified regions of interest; step 4, automatically blank sections of the grid which lie inside the body and compute overset connectivity weights. The finest off-body mesh spacing  $h$  is indicated in the lower plots.

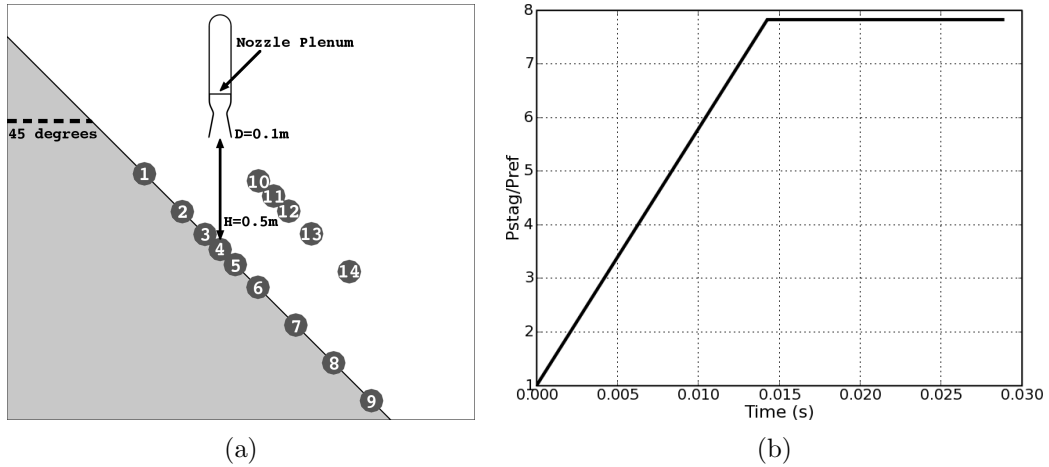


Figure 4. (a) Diagram of the IOP test case showing the two-dimensional nozzle, the 45-degree flat plate, and the 14 selected points for pressure extraction. (b) Time history of the stagnation pressure at the plenum of the nozzle.

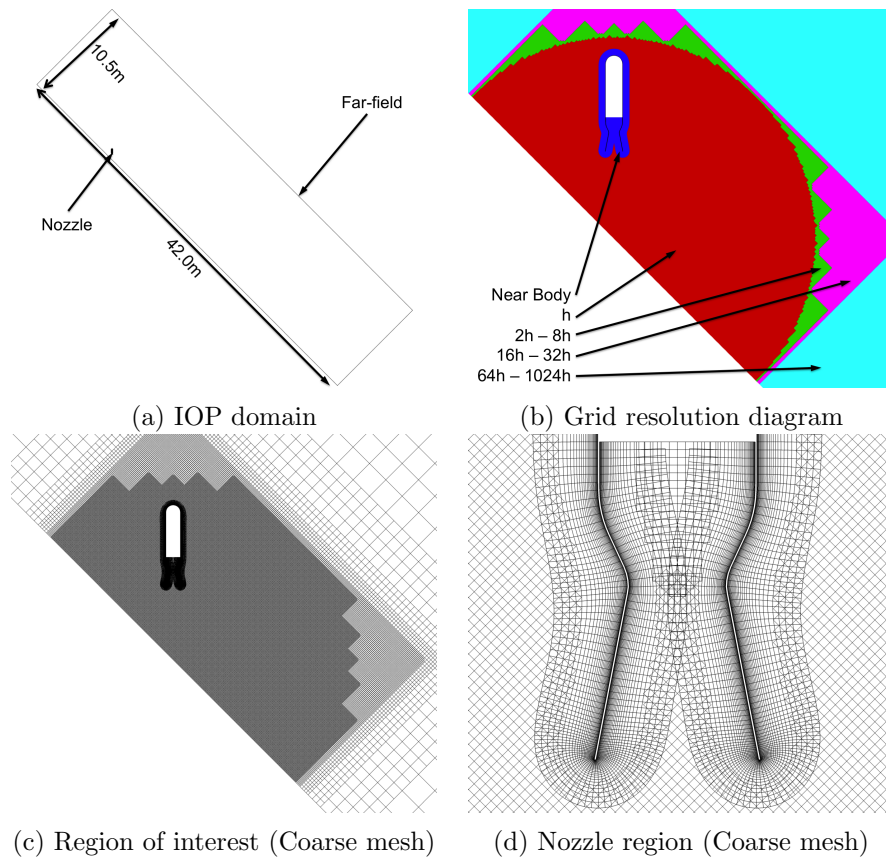


Figure 5. Description of grids used for IOP problem. (a) Extents of the solution domain. (b) Diagram showing the resolution used for specified regions. (c) Image of the coarse grid in the specified region of interest. (d) Close-up view of the nozzle section (Coarse grid).

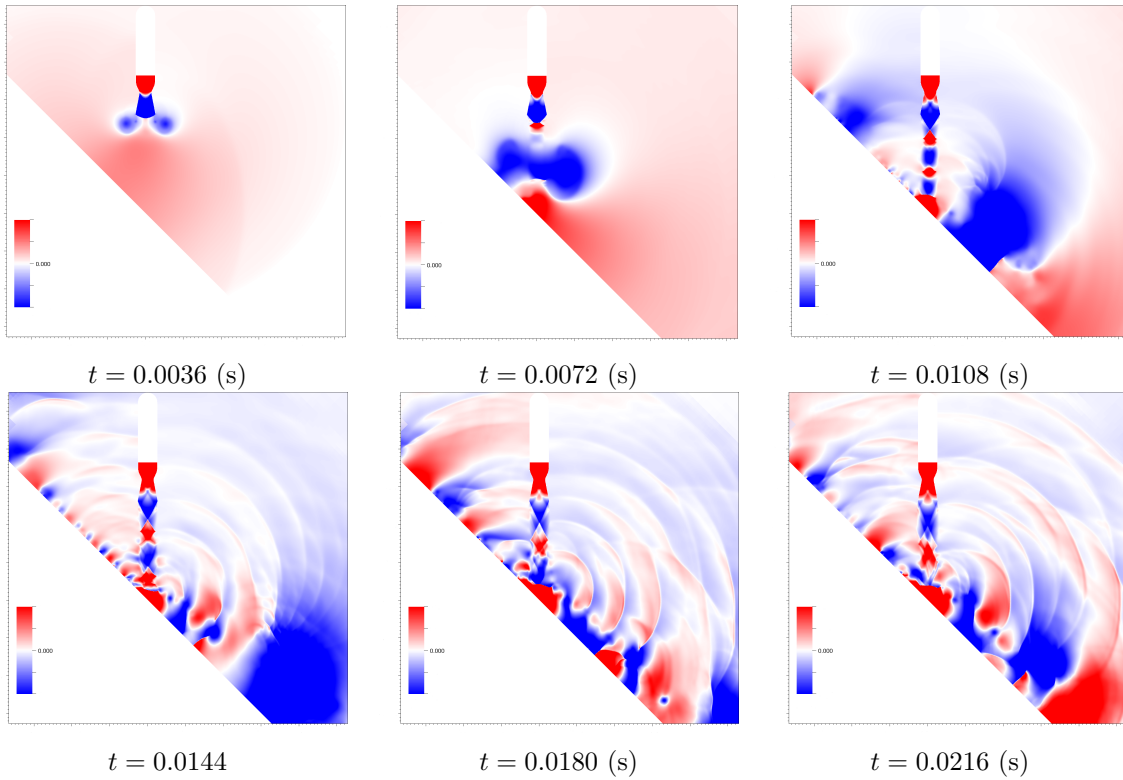


Figure 6. Time sequence of gauge pressure (psig) showing the IOP wave physics, the X- and Y-axis labels are in meters.

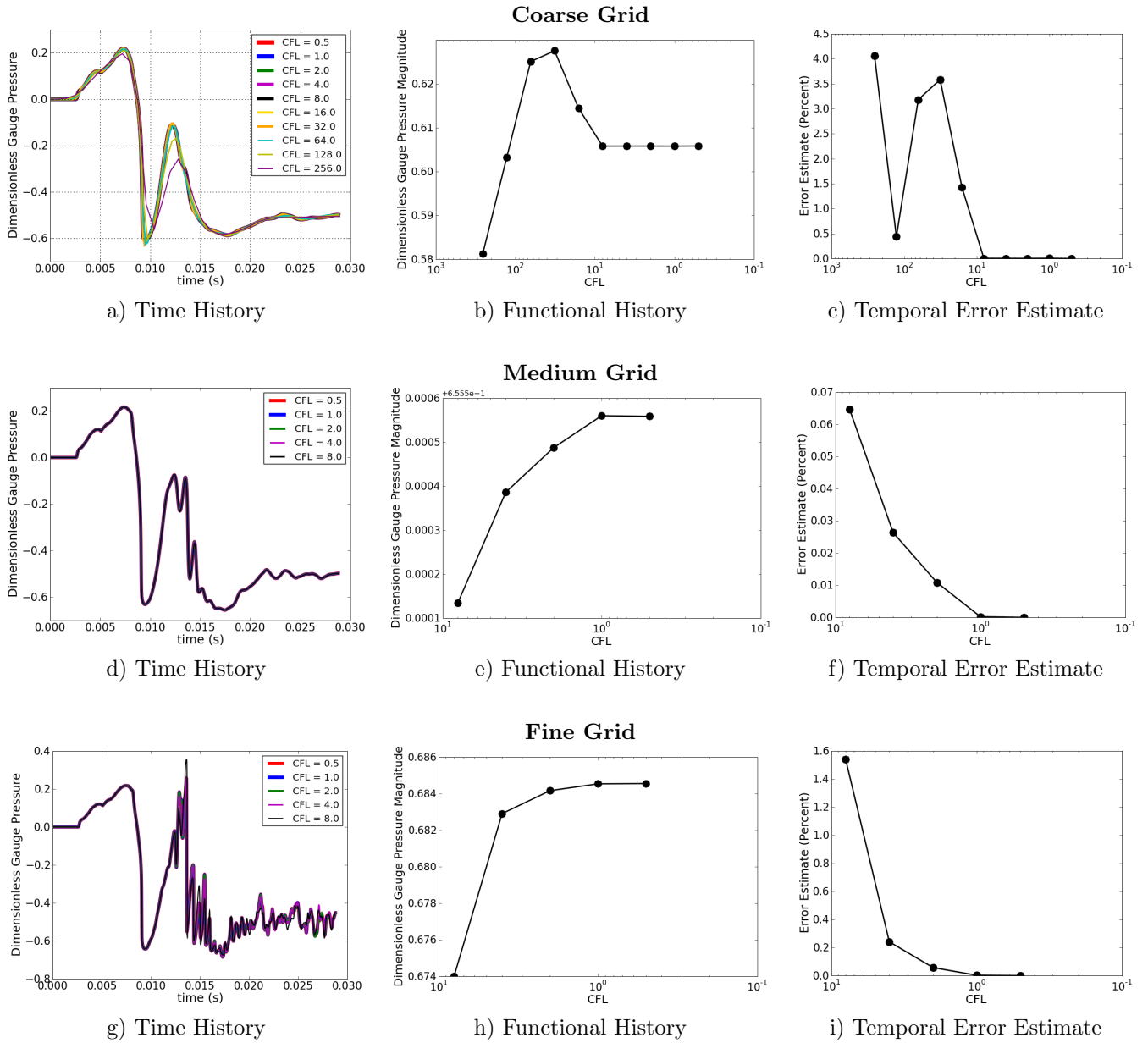
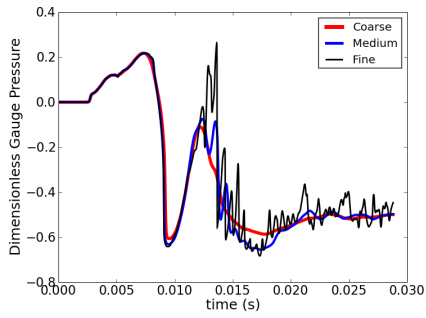
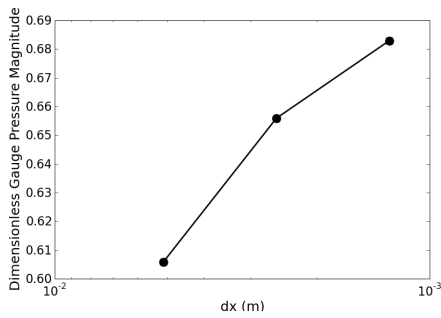


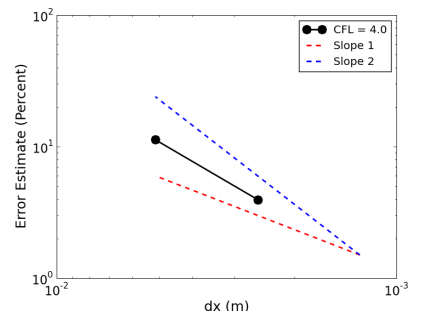
Figure 7. Time history of dimensionless gauge pressure for the IOP test problem at point location 6 along with functional convergence history and temporal error estimate as functions of  $CFL$ . Results for Coarse, Medium, and Fine grid resolutions are plotted in descending order. The  $CFL$  is plotted in reverse order on the  $x$ -axis so that the time-step is decreasing from left-to-right.



a) Time History

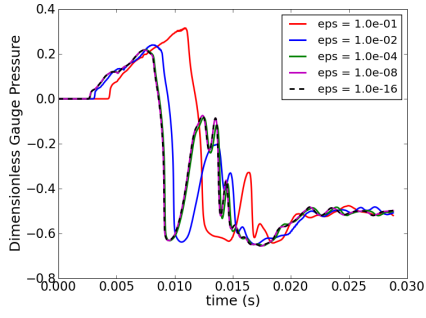


(b) Functional History

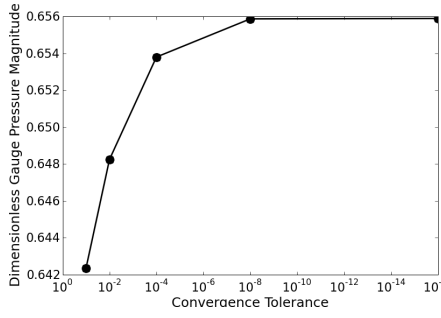


(c) Space-Time Error Estimate

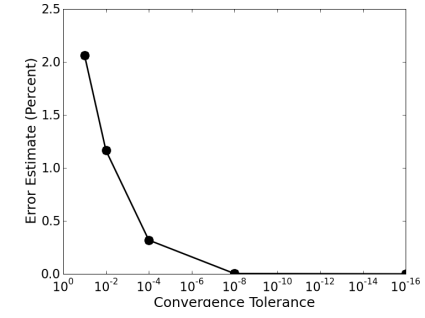
Figure 8. Space-time convergence results for the IOP wave problem at point location 6 using  $CFL = 4$ .



a) Time History



(b) Functional History



(c) Convergence Error Estimate

Figure 9. Convergence tolerance sensitivity results for the IOP wave problem at point location 6 using the medium mesh and  $CFL = 4$ .

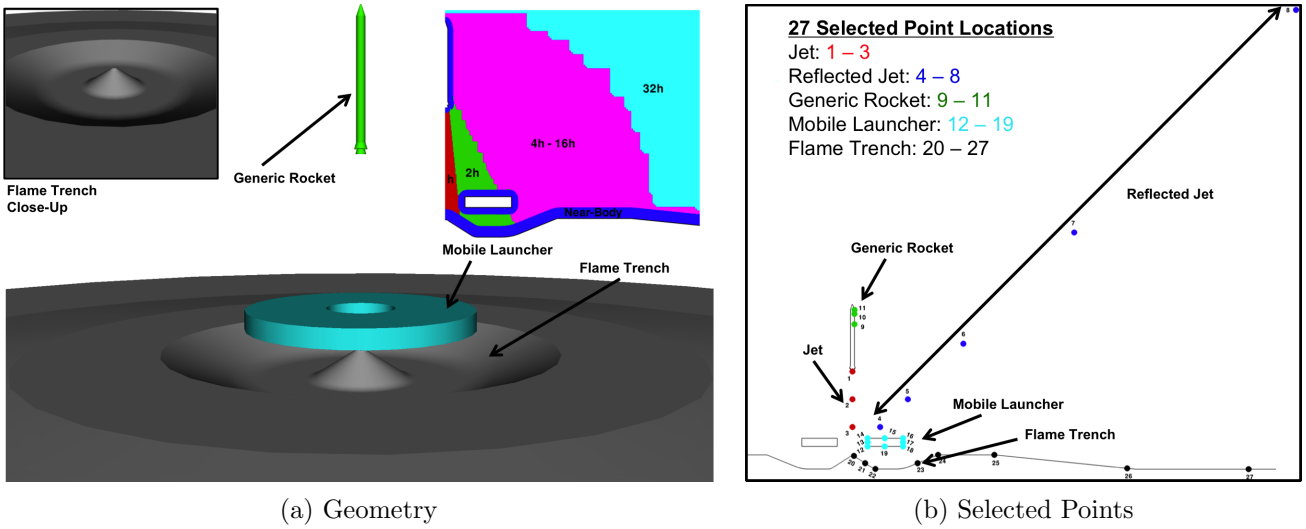


Figure 10. (a) Image showing the geometry of the launch acoustic test case which contains an axisymmetric rocket, mobile launcher and flame trench. A close-up of the flame trench is shown in the upper left, and a diagram showing the resolution used for specified regions in the upper right. (b) 27 selected point locations for pressure time-series extraction.

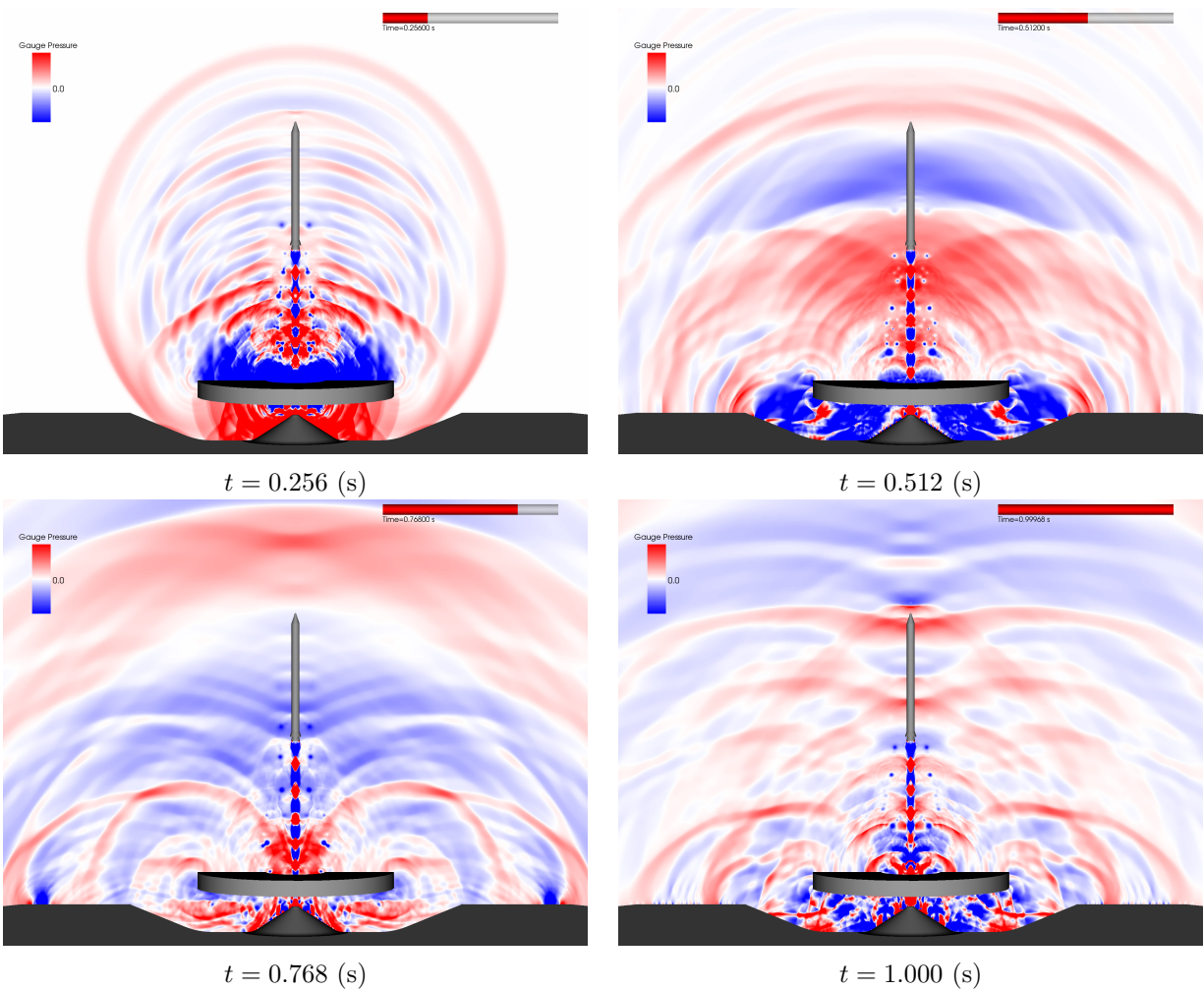


Figure 11. Time sequence of gauge pressure (psig) showing the launch acoustic initiation and propagation.

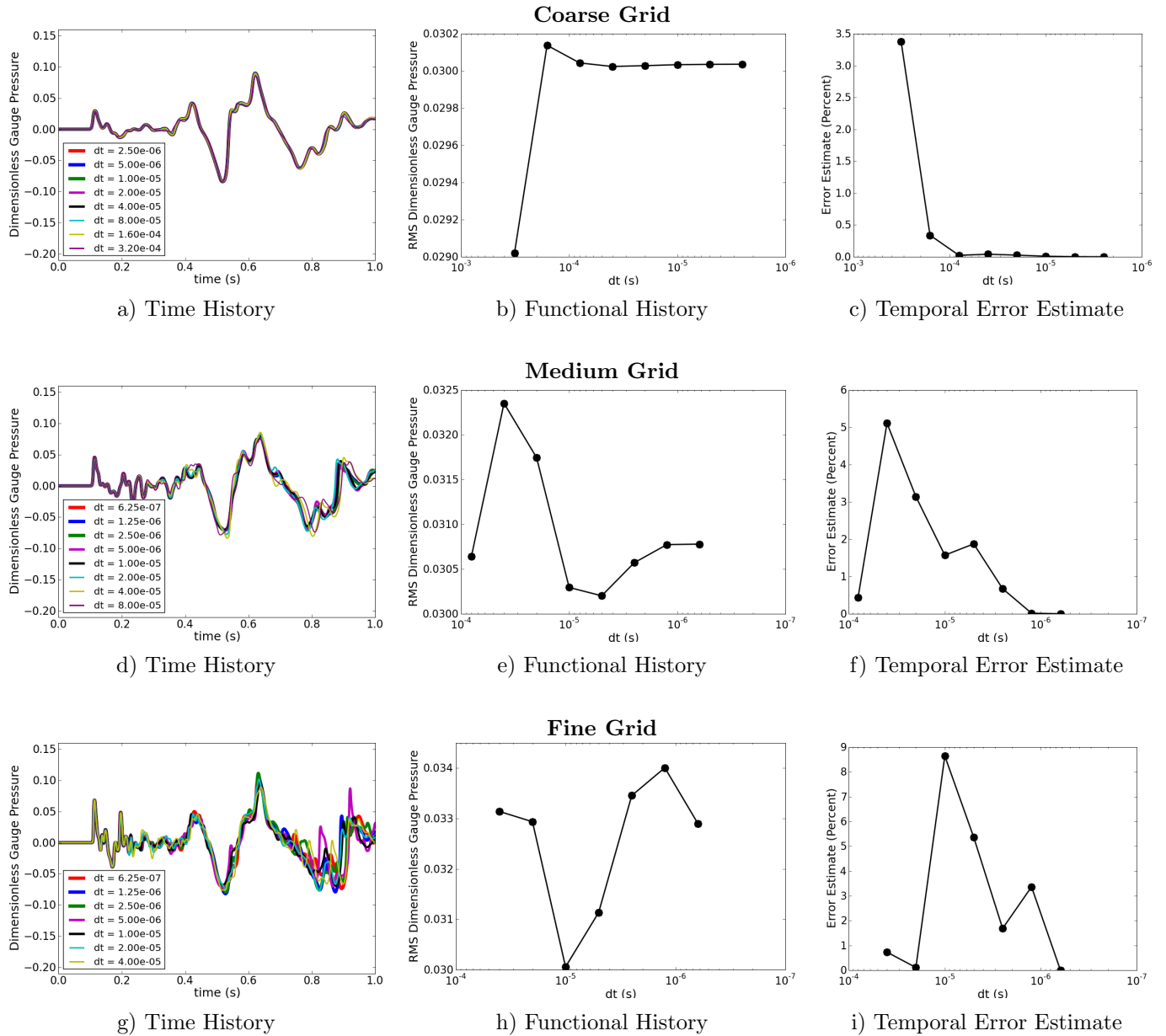


Figure 12. Time history of dimensionless gauge pressure for the launch acoustic test problem at point location 9 along with functional convergence history and temporal error estimate as functions of  $\Delta t$ . Results for Coarse, Medium, and Fine grid resolutions are plotted in descending order. The  $\Delta t$  is plotted in reverse order on the  $x$ -axis so that the time-step is decreasing from left-to-right.

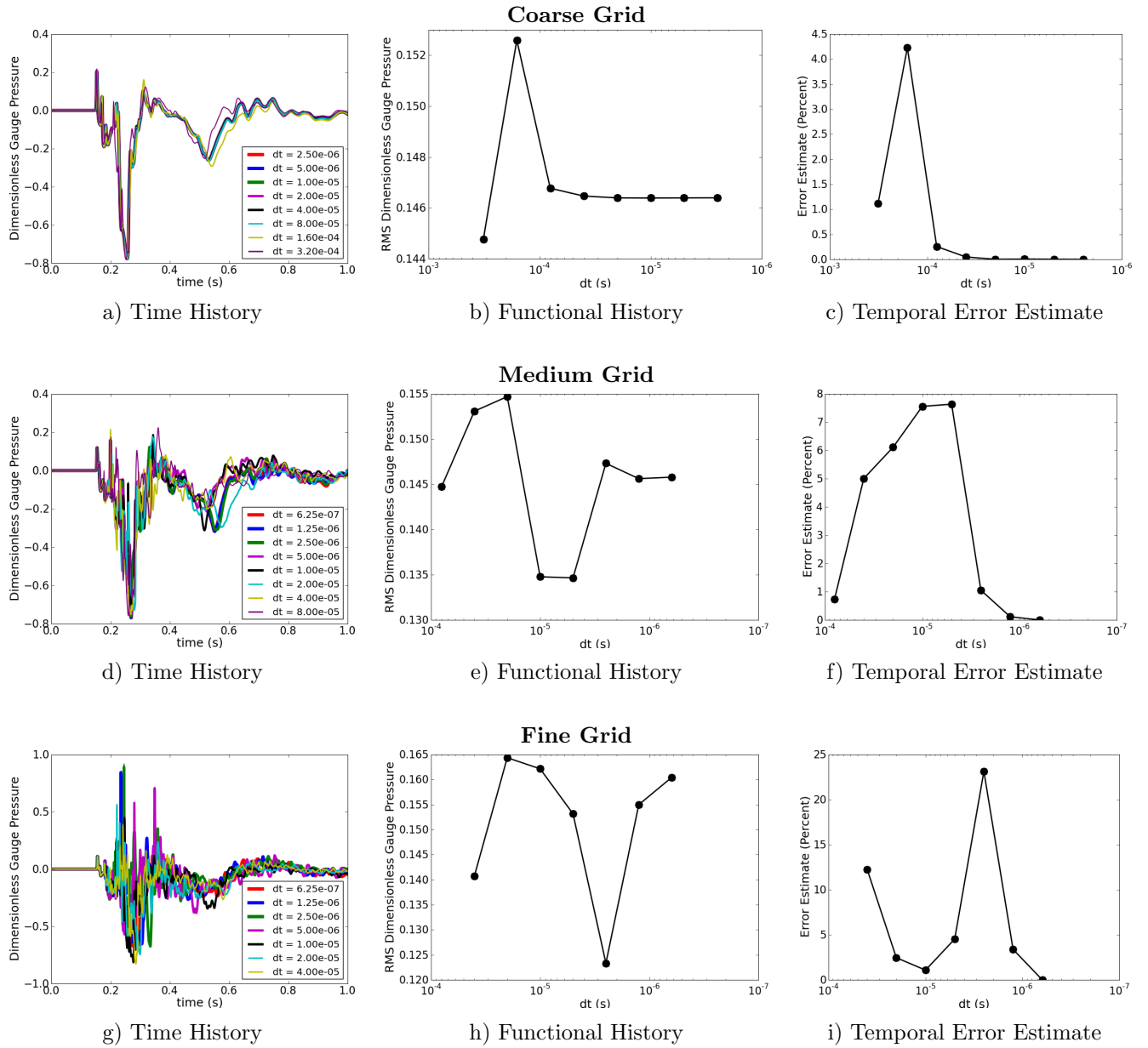


Figure 13. Time history of dimensionless gauge pressure for the launch acoustic test problem at point location 12 along with functional convergence history and temporal error estimate as functions of  $\Delta t$ . Results for Coarse, Medium, and Fine grid resolutions are plotted in descending order. The  $\Delta t$  is plotted in reverse order on the  $x$ -axis so that the time-step is decreasing from left-to-right.

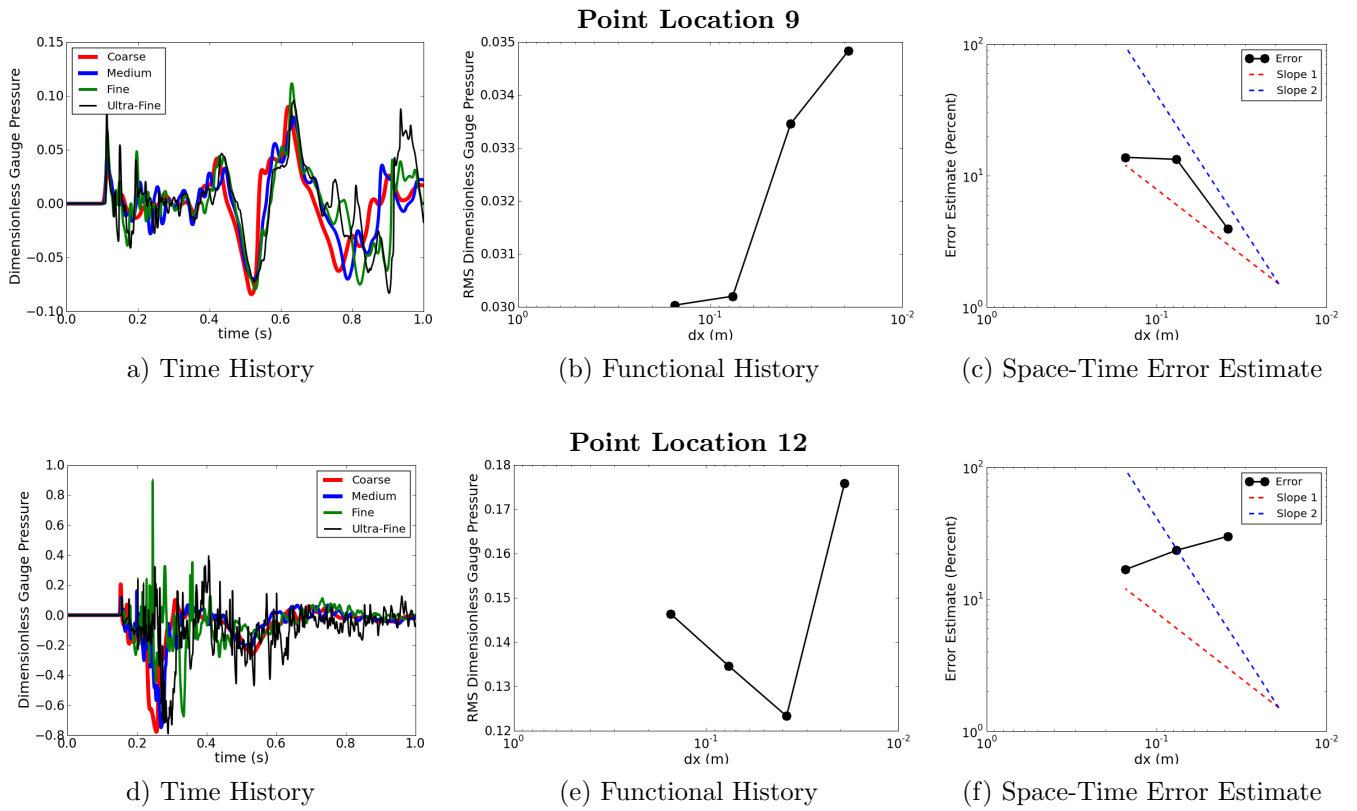


Figure 14. Space-time convergence results for the launch acoustic problem at point location 9 (top) and 12 (bottom) using the fixed ratio  $\Delta t/\Delta x = 1/15260$ .